

www.acsami.org Research Article

To Mimic Mechanical Properties of the Skin by Inducing Oriented Nanofiber Microstructures in Bottlebrush Cellulose-*graft*-diblock Copolymer Elastomers

Juan Zhang, Andrew N. Keith, Sergei S. Sheiko,* Xuehui Wang,* and Zhigang Wang*



Cite This: ACS Appl. Mater. Interfaces 2021, 13, 3278-3286



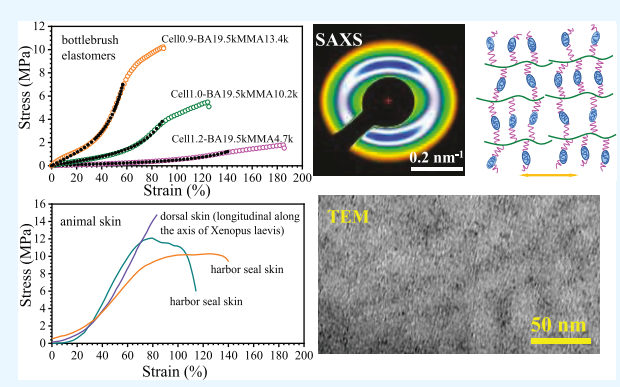
ACCESS

III Metrics & More

Article Recommendations

Supporting Information

ABSTRACT: Skin is a vital biological defense system that protects the body from physical harm with its unique mechanical properties attributed to the hierarchical organization of the protein scaffold. Developing a synthetic skinlike material has aroused great interest; however, replication of the skin's mechanical response, including anisotropic softness and strain-stiffening, is difficult to achieve. Here, to mimic the mechanical behaviors of skin, a reprocessable bottlebrush copolymer elastomer was designed with renewable and rigid cellulose as backbones; meanwhile, poly(*n*-butyl acrylate)-*b*-poly(methyl methacrylate) (PBA-*b*-PMMA) diblocks were designed as the grafted side chains. The so-made elastomers were subjected to a step-cyclic tensile deformation, by which the internal structures became oriented nanofibers and endowed stress—strain behaviors pretty much similar



to those of the real skin. Overall, our research work currently undertaken would be of great importance in the development of a series of biomimetic skinlike polymer materials.

KEYWORDS: bottlebrush copolymer, diblock copolymer side chains, microphase separation, cyclic tensile deformation, orientation

■ INTRODUCTION

Significant research has been conducted to program the physical properties of human and animal tissue 1-8 into synthetic materials for essential use in smart robots, wearable devices, 10 and bionic prostheses. 11 As a biological defense system, skin is the largest organ in humans and animals that quickly stiffens during deformation to protect the body from injury. 12,13 Among the three layers of skin (epidermis, dermis, and subcutaneous tissue), only the dermis layer supports skin's mechanical response, 1,14-17 which exhibits a highly nonlinear curve and a unique two-stage stress-strain variation during a uniaxial tensile deformation. $^{18-21}$ The first stage is a lowmodulus "toe" region, where crimpled collagen fibers unravel while the second stage is a high-modulus region where the collagen fibers are oriented and slide against each other. 18,19 The unique and universal mechanical performance of human and animal skins is correlated with routine living activities. On the one hand, the "toe" region is beneficial for a rapid and swift movement that consumes minimal energy; on the other hand, the high-modulus region is responsible for protecting the underlying tissues. Therefore, the goal of this study is to synthesize a series of materials that mimics skin's two-stage deformation, and the broad crossover state between the soft "toe" and strain-stiffening regions.

Many viscoelastic polymer networks have the potential to imitate skinlike mechanical characteristics, ^{19,22–27} for example,

rubber mimics skin indentation²⁶ and thermoplastic polyurethane mimics skin friction.²⁷ Recently, bottlebrush copolymer elastomers have received extensive attention due to their unique molecular conformation and mechanical behavior, but very few reports have demonstrated bottlebrush elastomers as potential materials for mimicking skin's tensile stress—strain. 28-35 Nevertheless, Sheiko et al. designed self-assembled linear-bottlebrush-linear ABA-type triblock copolymer elastomers that could mimic the stimuli-responsive structural coloration and mechanical response of chameleon skin.³⁶ The bottlebrush B block provided a low modulus for the polymer network, while the microphase separation between the linear and brush blocks enhanced its strain-stiffening behavior.³⁶ However, the mechanical strength of these thermoplastic elastomers was considerably low compared to that of ordinary skin. Recently, we have reported the synthesis of chemically crosslinked elastomers consisting of rigid cellulose backbone chains and elastic grafted polyisoprene

Received: December 3, 2020 Accepted: December 29, 2020 Published: January 8, 2021





(PI) side chains that mimicked the microstructure and mechanical properties of resilin and human skin. ^{28,37} Although the mechanical response for these elastomers could match modulus and strength of human skin, an obvious drawback of less processability remained due to chemical crosslink.

In our current study, we have synthesized well-designed bottlebrush cellulose-graft-diblock copolymers (Cell-g-PBA-b-PMMA) via an atom-transfer radical polymerization utilizing a halide-exchange technique, in which cellulose is the rigid backbone and poly(n-butyl acrylate)-b-poly(methyl methacrylate) (PBA-b-PMMA) diblock copolymer side chains are grown from the cellulose.33 In these bottlebrush copolymers, microphase separation occurs due to immiscibility between PBA and PMMA blocks, leading to the formation of PMMA hard domains dispersed in the PBA matrix. The advantage of these bottlebrush graft copolymers over simple diblock copolymers is that the soft PBA matrix is strung together through rigid cellulose backbones and further connected by physically cross-linked PMMA domains, yielding a fully conjugated system integrating softness and rigidity (initial softness and strain-adaptive stiffening). The hard PMMA domains would contribute to the tensile strength, while the soft PBA matrix to the low modulus and recovery.³⁸ As a result, extending and aligning the hard PMMA domains into fiber-like structures allow mimicking of skin's anisotropic mechanical response.^{37,39} It should be emphasized that PMMA forms physical cross-linking points, which enable skinlike materials liable to process in various shapes and sizes.

■ EXPERIMENTAL SECTION

Synthesis of Bottlebrush Cell-g-PBA-b-PMMA Copolymer Elastomers. The synthesis of Cell-g-PBA-b-PMMA has just been reported in a short communication.³³ It is emphasized that when cellulose-graft-poly(n-butyl acrylate) (Cell-g-PBA) was considered to play the role as the macromolecular initiator to initiate the polymerization of the second monomer, methyl methacrylate (MMA), a halide-exchange technique must be employed for the successful synthesis of bottlebrush Cell-g-PBA-b-PMMA copolymers.

Thermogravimetric Analysis (TGÅ). TGA thermograms were collected using a TG209 F3 Tarsus thermogravimetric analyzer (NETZSCH Instrument) with a heating rate of 20 °C/min under a nitrogen atmosphere from room temperature to 100 °C. Samples were held at 100 °C for 30 min, and then cooled to 40 °C again at a rate of 20 °C/min. Subsequently, the samples were heated from 40 to 800 °C with a programmed temperature increment of 10 °C/min.

Dynamic Mechanical Analysis (DMA). Dynamic mechanical properties were conducted using a DMA Q800 (TA Instruments) under a nitrogen atmosphere. The DMA measurements were carried out using dog-bone specimens (2 mm × 0.3 mm × 35 mm) and heated from -90 to 200 °C at a heating rate of 3 °C/min while maintaining a constant 1 Hz frequency in the tensile mode. Note that a 0.2% strain was applied in the tests.

Mechanical Properties Test. The films for the mechanical properties test were prepared by dissolving the copolymers in THF and then casting them in a Teflon mold. All film samples were annealed at 150 °C for 24 h and then cut into dog-bone specimens with a width of 2 mm, length of 35 mm, and thickness of 0.3–0.5 mm. The tensile deformation tests were performed on a Suns Model UTM2502 machine kept at a relatively constant ambient temperature (23 \pm 1 °C). The cross-head speed was 5 mm/min. The tensile deformation curves for the processed bottlebrush Cell-g-PBA-b-PMMA copolymer elastomers mimicking the mechanical properties of skin were obtained after the step-cyclic tensile deformation, and the elastic recovery (ER) values were derived from the stress—strain curves of the step cycles. 37,39

Small-Angle X-ray Scattering (SAXS). The SAXS measurements on the pristine and processed film samples were collected on a Mar165 CCD detector at beamline BL16B1 at the Shanghai Synchrotron Radiation Facility (SSRF). The wavelength of the X-ray was 0.124 nm. The sample-to-detector distance was 2001 mm. The SAXS patterns were corrected for background scattering.

Transmission Electron Microscopy (TEM). The internal microstructures of the pristine and processed bottlebrush cellulose-graft-diblock copolymers were observed using a Hitachi HT7700 TEM operating at an acceleration voltage of 80 kV. The samples were cut into slices of approximately 70 nm using a microtome at $-120\,^{\circ}\text{C}$, and the slices were collected on copper meshes. Subsequently, the copper meshes carrying the slices were exposed to ruthenium tetroxide (RuO₄) vapor for staining of 2 h.

■ RESULTS AND DISCUSSION

Mechanical Properties of Bottlebrush Cellulose-graft-diblock Copolymer Elastomers Mimicking Human or Animal Skin. A series of bottlebrush copolymers (Cell-g-PBA-b-PMMA) consisting of a cellulose backbone chain with grafted diblock copolymer side chains (PBA-b-PMMA) were synthesized by successive atom transfer radical polymerization (ATRP) utilizing a halide-exchange technique. The synthetic formulae, characteristics, and schematic of the chain structure of Cell-g-PBA-b-PMMA samples can be found in Table 1 of our recent paper³³ and in Figure 1a (inset),

Table 1. Mechanical Properties of Cell-g-PBA-b-PMMA Copolymers Relative to Human and Animal Skins

sample	$E (MPa)^a$	β^a	E_0 (MPa)
Cell0.9-BA19.5kMMA13.4k	1.1	0.64	5.9
Cell1.0-BA19.5kMMA10.2k	0.8	0.47	2.1
Cell1.2-BA19.5kMMA4.7k	0.3	0.29	0.5
human abdominal skin	0.4	0.52	1.2

^aThe structural modulus $E \sim 1/(n_{\rm bb}(n_{\rm sc}+1))$ and nonlinear strainstiffening parameter $\beta=\langle R_{\rm in}^2/R_{\rm max}^2$ are fitting parameters in

$$\sigma_{\text{true}}(\lambda) = \frac{E}{9}(\lambda^2 - \lambda^{-1}) \left[1 + 2 \left(1 - \frac{\beta(\lambda^2 + 2\lambda^{-1})}{3} \right)^{-2} \right]$$

The apparent Young's modulus can be determined either as the tangent of a stress–strain curve at $\lambda \to 1$ or from the fitting equation at $\lambda = 1$ as $E_0 = E/3(1 + 2(1 - \beta)^{-2})^{.45}$

where Cell1.0-BA19.5kMMA10.2k, for instance, is defined by BA and MMA molecular mass values, respectively, and the cellulose mass percent content follows "Cell". Meanwhile, a linear diblock copolymer, poly(n-butyl acrylate)-block-poly(methyl methacrylate) (PBA-b-PMMA, BA23.1kMMA10.9k), was also synthesized as a control (Figure S1 in the Supporting Information), in which the glass transition temperature (T_g) of the PBA block is -46.4 °C and that of PMMA is 108.7 °C, measured by differential scanning calorimetry (DSC). The far apart T_g 's of PBA and PMMA blocks for both Cell-g-PBA-b-PMMA and PBA-b-PMMA demonstrate the successful synthesis of bottlebrush cellulose-graft-diblock copolymers. 33

The thermal stability for bottlebrush copolymers (Cell-g-PBA-b-PMMA) is also evaluated by thermogravimetric analysis (TGA). The TGA and derivative thermogravimetry (DTG) curves for cellulose, Cell-BiB, Cell-g-PBA, and Cell1.2-BA19.5kMMA4.7k are shown in Figures 1a and S2, respectively. It can be seen that the thermal degradation of cellulose occurs in the range of 260–390 °C using a one-step

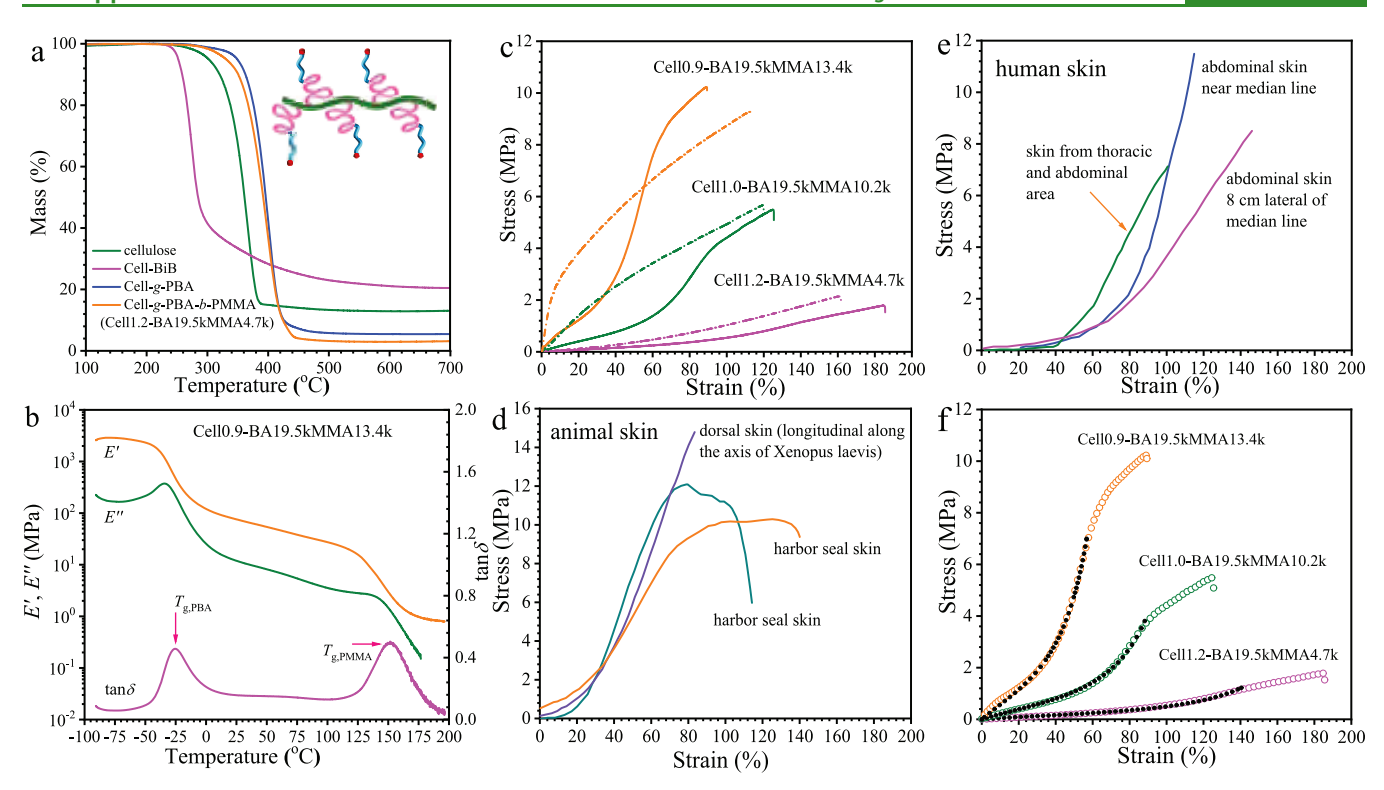


Figure 1. Dynamic thermomechanical behavior and skinlike stress—strain behavior of bottlebrush Cell-g-PBA-b-PMMA copolymers. (a) TGA curves and (b) changes in the storage modulus (E'), loss modulus (E''), and loss tangent (tanδ). (c) Mimicking skin's mechanical properties for bottlebrush cellulose-graft-diblock copolymer elastomers, illustrated by monotonic nominal stress—strain curves (solid lines) of Cello.9-BA19.5kMMA13.4k (orange), Cell1.0-BA19.5kMMA10.2k (green), and Cell1.2-BA19.5kMMA4.7k (magenta) after cyclic tensile deformation of 6, 4, and 7 cycles, respectively (dash-dot lines for pristine samples). (d) Monotonic nominal stress—strain curves for human skin (skin from the thoracic and abdominal area, ¹⁹ and abdominal skin near the median line, and abdominal skin 8 cm lateral of the median line. ⁴⁰ (e) Monotonic nominal stress—strain curves for the animal skin (dorsal skin longitudinal along the animal axis of Xenopus laevis, ⁴¹ and harbor seal skins. ⁴² (f) Fitting (black lines) of step-cycled Cell-g-PBA-b-PMMA copolymers using an elastic model. ⁴⁵ The stress in all of the plots represents engineering stress.

procedure, displaying a maximum degradation temperature at 366 °C and yielding a residual mass of 13 wt %. Thermal stability of Cell-BiB is significantly deteriorated due to cellulose acylation modification, reducing the maximum degradation temperature to 274 °C and the degradation range to 220-320 °C with a residual mass of 20 wt %. This result can be explained by the introduction of a relatively unstable brominated alkyl unit in cellulose. On the other hand, the thermal stability of cellulose-graft-diblock copolymers is significantly improved, for example, the maximum degradation temperatures for Cell-g-PBA and Cell1.2-BA19.5kMMA4.7k increase to 401 and 398 °C, respectively. In addition, the onset degradation temperatures for both samples are also much higher than those of cellulose and Cell-BiB. Together, the TGA and DTG curves for Cell1.0-BA19.5kMMA10.2k and Cell0.9-BA19.5kMMA13.4k are also summarized in Figure S3, proving that bottlebrush Cell-g-PBA-b-PMMA copolymers have significantly enhanced thermal stability and could serve as superior elastomers in many end uses.

The dynamic thermomechanical behavior of bottlebrush Cell-g-PBA-b-PMMA copolymers was examined by dynamic mechanical analysis (DMA). The DMA curves in Figure 1b show the changes in the storage modulus (E'), loss modulus (E''), and loss tangent $(\tan\delta)$, with increasing temperature for Cell0.9-BA19.5kMMA13.4k at a heating rate of 3 °C/min under a nitrogen atmosphere in a tensile mode. Two distinct $\tan\delta$ peaks are first observed, which correlate with the glass

transition temperatures of PBA and PMMA blocks ($T_{\rm g,PBA}$ = -25.4 and $T_{\rm g,PMMA}$ = 151.1 °C) and confirm PBA and PMMA microphase separation in the grafted side chains (see inset in Figure 1a). Therefore, soft PBA blocks with low $T_{\rm g}$ can endow elasticity, while hard PMMA blocks with high $T_{\rm g}$ endow stiffness and strength to bottlebrush Cell-g-PBA-b-PMMA copolymers. A second feature detected is that the storage modulus broadly covers from 117 to 16.6 MPa in a wide temperature range from -2.7 to 123 °C, which allows its practical applications at ambient temperatures (E' = 80 MPa at 23.5 °C). The above thermal and thermomechanical behaviors for the synthesized bottlebrush Cell-g-PBA-b-PMMA copolymers warrant our further study of their skinlike mechanical properties.

Figure 1c-f shows tensile responses of bottlebrush Cell-g-PBA-b-PMMA copolymer elastomers along with various animal and human skins (Figure 1d,e). The dash-dot lines represent the stress-strain curves of the as-prepared bottlebrush Cell-g-PBA-b-PMMA copolymer elastomers, in which the "toe" and "tough" regions are not observed in Cell0.9-BA19.5kMMA13.4k and Cell1.0-BA19.5kMMA10.2k and the "tough" region is not observed in Cell1.2-BA19.5kMMA4.7k. After physically reprocessing the samples through cyclic tensile deformation, they demonstrate both "toe" and "tough" regions, which mimic skin's mechanical performance (solid lines in Figure 1c). This cyclic deformation leads to the reconstruction of the internal nanosized

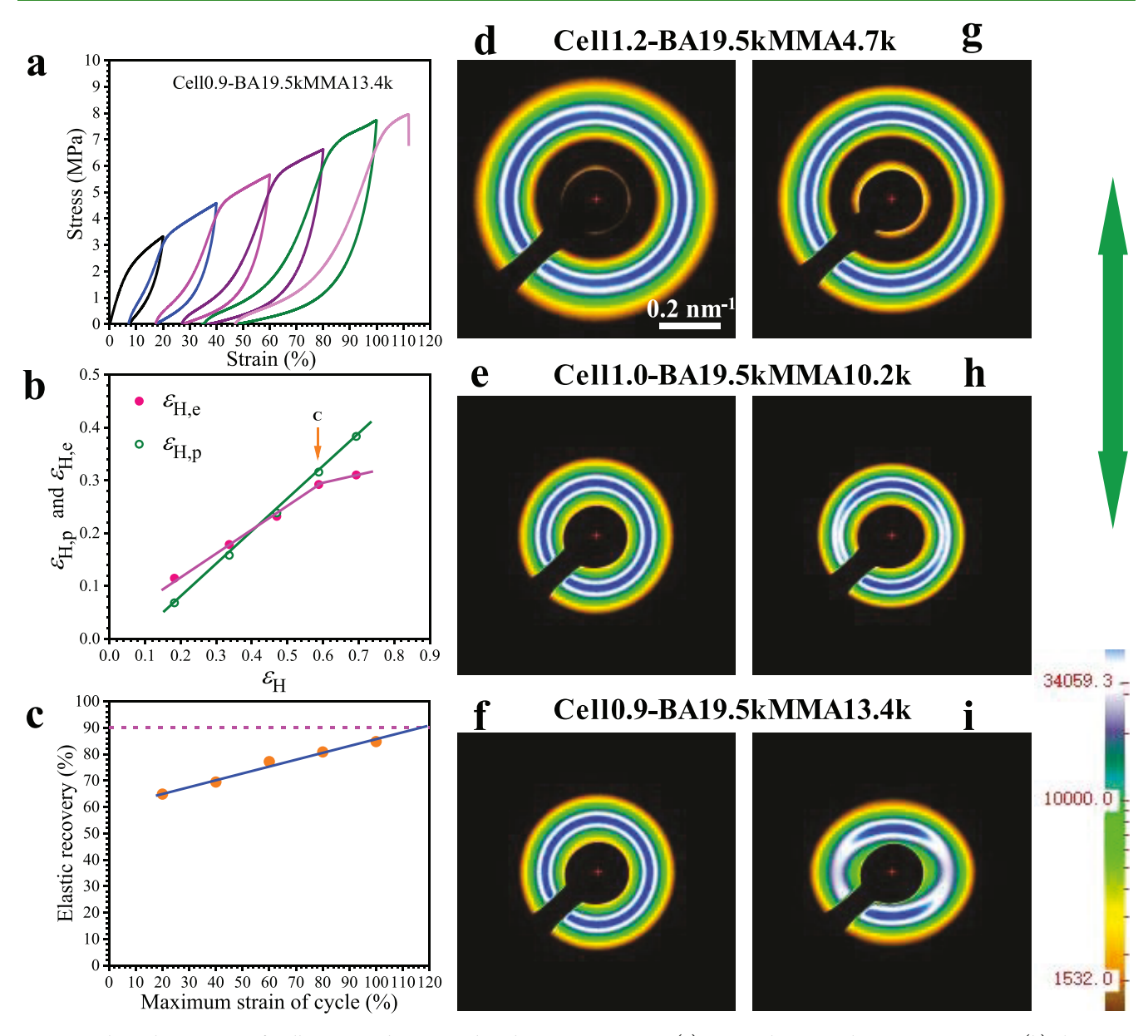


Figure 2. Physical processing of Cell0.9-BA19.5kMMA13.4k and 2D SAXS patterns. (a) Step-cyclic nominal stress—strain curves, (b) changes in the true plastic strain, $\varepsilon_{\rm H,p}$, and true elastic strain, $\varepsilon_{\rm H,e}$, with maximum true strain, $\varepsilon_{\rm H}$, in each cyclic step and (c) change in the elastic recovery with maximum strain in each cyclic step during the step-cyclic tensile deformation for Cell0.9-BA19.5kMMA13.4k. The critical strain at point C is marked in (b). Two-dimensional (2D) SAXS patterns for pristine samples (d–f) and the processed samples by step-cyclic tensile deformation (g–i). Olive color double-head arrow at the right side indicates the tensile direction. Scale bar in (d) is applicable to all other SAXS patterns.

microstructures, which will be discussed below. Visually comparing these processed samples to tissue reveals that Cell0.9-BA19.5kMMA13.4k behaves most closer to the skin as shown in Figure 1d,e. Cell1.0-BA19.5kMMA10.2k and Cell1.2-BA19.5kMMA4.7k show relatively modest mechanical strengths and high elongations at break, but they are still able to mimic the mechanical properties of some types of skins, such as those on the back of rats and on the abdomen of pigs. 43,44 As a control, the stress-strain curve for linear PBA-b-PMMA diblock copolymer (BA23.1kMMA10.9k) is shown in Figure S4. Although its molecular mass (Figure S5) is close to that of the grafting side chains of Cell1.0-BA19.5kMMA10.2k, the mechanical strength is far inferior to that of Cell1.0-BA19.5kMMA10.2k. This comparison indicates that the underlying bottlebrush architecture plays a key role in achieving skinlike mechanical responses. Previous studies

showed that the nonlinear elasticity of biological network and gel and polymer network is universal in a certain strain range.⁴⁵ To better quantify the resulting mechanical properties of the processed Cell-g-PBA-b-PMMA copolymers, we utilize a fitting model that characterizes the nonlinear "toe" region for elastic systems shown as dotted lines in Figure 1f. 45 Importantly, the fitting equation precisely fits the entire elastic "toe" region and extracts two elastic parameters: Young's modulus (E_0) and strain-stiffening parameter (β) , which, respectively, describe the initial slope of the curve and the subsequent nonlinear curvature. The structural modulus E is determined by the density and conformation, and the strainstiffening parameter β depends on the potential extensibility of the network. Thus, the model proves that the bottlebrush cellulose-graft-diblock copolymer elastomers have a similar nonlinear elasticity to a biological network. These extracted

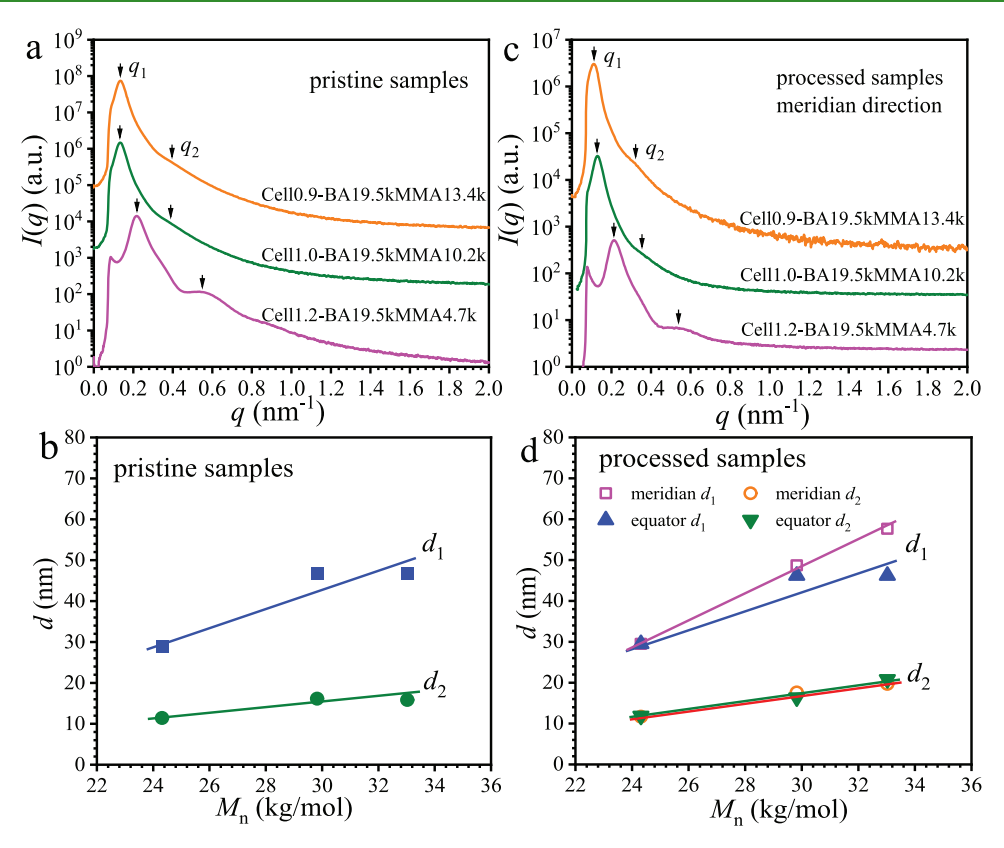


Figure 3. SAXS intensity profiles and variation of interdomain distances. I(q) vs q for (a) pristine and (c, meridian direction) the processed Cell1.2-BA19.5kMMA4.7k, Cell1.0-BA19.5kMMA10.2k, and Cell0.9-BA19.5kMMA13.4k copolymers. Changes in the interdomain distances, d_1 and d_2 , with the number-average molecular mass of the grafted diblock copolymer chains for (b) pristine and (d) the processed bottlebrush Cell-g-PBA-b-PMMA copolymer elastomers.

parameters from the Cell-g-PBA-b-PMMA copolymers (Figure 1c) along with representative animal skin (Figure 1d) and human skin (Figure 1e) are shown in Table 1. We emphasize that all polymers, including plastics, rubber, elastomers, filled rubber composites, etc., do not mimic the two-phase mechanical performance of human or animal skin. Typically, the "toe" region does not exist for polymers and the "tough" region occurs at a much large strain for soft rubbers with embedded fibers, which are both distinct from the performance of the skin.

Step-Cyclic Tensile Deformation Physical Process to Accomplish Skinlike Mechanical Properties. The nominal stress-strain curves shown in Figure 1 illustrate that bottlebrush Cell-g-PBA-b-PMMA copolymers can have quite different mechanical behaviors compared to pristine samples. This transformation is simply accomplished by applying a physical procedure, called a step-cyclic tensile deformation. Figure 2a displays cyclic steps of stress-strain curves for Cell0.9-BA19.5kMMA13.4k with the strain of each cycle designed as 20, 40, 60, 80, and 100%. Both stress-softening, called the Mullins effect, 46 and hysteresis are observed in each cycle caused by irreversible permanent plastic deformation. As shown in Figure 2b, the maximum true strain (ε_H) of each cycle can be separated into irreversible true plastic strain $(\varepsilon_{\rm H,p})$ and reversible true elastic strain $(\varepsilon_{\rm H,e})$. The irreversible true plastic strain $(\varepsilon_{\rm H,p})$ increases linearly with the true strain $(\varepsilon_{\rm H})$, while there exists a critical strain at point C ($\varepsilon_{\rm H}$ = 0.59) for reversible true elastic strain ($\varepsilon_{\mathrm{H.e}}$), which is possibly correlated with the deconstruction of PMMA phase domains at the high strain range.⁴⁷ The irreversible plastic deformation keeps

rearranging the internal microstructures in each cycle, leading to the gradually enhanced elastic recovery, as demonstrated in Figure 2c. The elastic recovery increases from 65 to 85%, approaching 90% as predicted at the maximum strain of 120% and indicated by the pink dotted line. Therefore, after processing the pristine samples by the step-cyclic tensile deformation, the obtained bottlebrush copolymer elastomers exhibited different mechanical behaviors as shown in Figure 1c, which mimic that of human and animal skins.

Internal-Oriented Microstructures Resulted from Step-Cyclic Tensile Deformation Process. The skinlike mechanical performance may be attributed to the unique internal microstructures in the processed bottlebrush copolymer elastomers. To prove this, small-angle X-ray scattering (SAXS) was performed. Figure 2d-i shows the respective 2D SAXS patterns for Cell1.2-BA19.5kMMA4.7k, Cell1.0-BA19.5kMMA10.2k, and Cell0.9-BA19.5kMMA13.4k in pristine and step-cyclic tensile deformation samples. The SAXS patterns displayed in Figure 2d-f are isotropic, indicating that the internal microstructures are randomly oriented in the samples. The SAXS patterns displayed in Figure 2g-i for Cell1.0-BA19.5kMMA10.2k and Cell0.9-BA19.5kMMA13.4k show two arcs on the meridian direction, while for Cell1.2-BA19.5kMMA4.7k the SAXS pattern does not show any visible orientation, indicating that the short PMMA block might not provide sufficient relaxation time for maintaining the oriented microstructures. The meridian arcs in the SAXS patterns for Cell1.0-BA19.5kMMA10.2k and Cell0.9-BA19.5kMMA13.4k samples demonstrate that the microdomains are actually oriented perpendicular to the stretching direction, marked by an olive color double-head arrow on the right side. The orientation of cellulose backbones could not be detected using SAXS due to their low content. The oriented microstructures in the processed bottlebrush Cell-g-PBA-b-PMMA copolymer elastomers are strongly proved to be responsible for mimicking the mechanical properties of skin.

To obtain quantitative information, the integrated SAXS intensity profiles are extracted from the 2D SAXS patterns shown in Figure 2. The SAXS intensity profiles (I(q) vs q) for pristine Cell1.2-BA19.5kMMA4.7k, Cell1.0-BA19.5kM-MA10.2k, and Cell0.9-BA19.5kMMA13.4k copolymers are shown in Figure 3a, while the SAXS intensity profiles along the meridian and equator direction for the processed copolymers are shown in Figures 3c and S6, respectively. All of the intensity profiles exhibit a primary SAXS peak at q_1 , which is related to the interdomain distance for their cylindrical microstructure.³³ Besides the primary peak for each profile, a weak secondary shoulder is visible on each profile marked as q2. The secondary peak looks relatively clear for Cell1.2-BA19.5kMMA4.7k with the respective q_1 and q_2 values of 0.22 and 0.55 nm⁻¹, corresponding to the interdomain distance of 28.9 and 11.5 nm. Typically ordered microstructures, such as lamellar or hexagonal types, cannot be assigned by the relationship between these two values. Therefore, it is predicted that two types of interdomain distances in the samples might exist, which is observed by TEM in a later section. For the pristine and processed bottlebrush copolymers, the SAXS profiles do not show obvious differences in shape. The subtle changes in the microstructures due to tensile deformation are further analyzed by plotting the changes in the interdomain distance among these samples. Figure 3b,d shows the changes in the two interdomain distances, d_1 and d_2 , with the number-average molecular mass of the grafted diblock copolymer chains for the pristine and the processed bottlebrush Cell-g-PBA-b-PMMA copolymer elastomers. It can be seen that the interdomain distances, d_1 and d_2 , both increase with increasing graft molecular mass, with a more significant increase in d_1 than in d_2 (Figure 3b). The cyclic tensile deformation also alters d_1 although the d_2 remains constant, as d_1 becomes larger for the microstructures perpendicular to the meridian direction than for the equator direction (Figure 3d). The enlargement in d_1 along the meridian direction can be gradually enhanced by increasing the PMMA block length, which is caused by the slow relaxation time of the hard PMMA block.

The SAXS arcs in the meridian direction shown in Figure 2h,i can be used to quantitatively assess the degree of orientation of the microstructures in the processed samples. For this purpose, the azimuthal intensity profiles need to be extracted from the SAXS patterns. Figure 4 shows the azimuthal intensity profiles taken at the primary SAXS peak position q_1 for six SAXS patterns in Figure 2. All pristine samples show flat azimuthal intensity profiles in Figure 4a, indicating that no structural orientation exists in these samples. However, the processed samples Cell1.0-BA19.5kMMA10.2k and Cell0.9-BA19.5kMMA13.4k do show two main peaks approximately at 0 and 180° on their azimuthal intensity profiles. The processed sample Cell1.2-BA19.5kMMA4.7k does not show these peaks due to the rapid relaxation of the grafted side chains. The degree of orientation can be characterized by the orientation parameter $\langle P_2 \rangle$, while the orientation factor $\langle\cos^2\phi\rangle_{\rm Av}$ can be calculated using the following equation 48

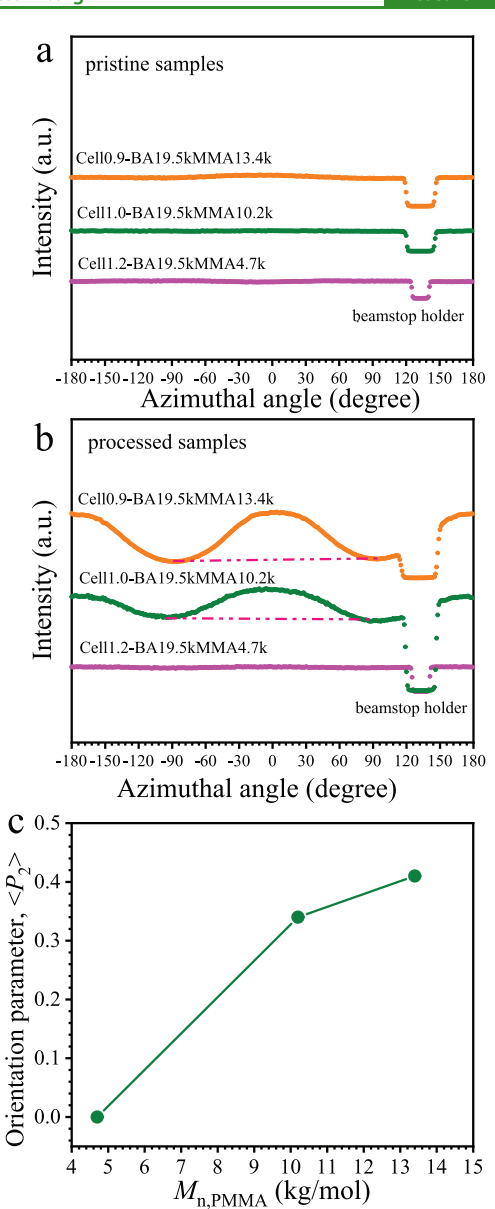


Figure 4. Azimuthal intensity profiles and the change in the orientation parameter. Azimuthal intensity profiles taken at the primary peak position from SAXS patterns for (a) pristine and (b) the processed bottlebrush Cell-g-PBA-b-PMMA copolymer elastomers. The intensity dip in the angle range of about 120–150° is due to the beamstop holder. (c) The change in the orientation parameter with the molecular mass of the PMMA block.

$$\langle \cos^2 \phi \rangle_{Av} = \int_0^{\pi/2} I(\phi) \cos^2 \phi \sin \phi \, d\phi / \int_0^{\pi/2} I(\phi) \sin \phi \, d\phi$$

$$d\phi \qquad (2)$$

where $I(\phi)$ is the SAXS intensity at the azimuthal angle ϕ , and the orientation parameter $\langle P_2(\cos\phi) \rangle$ is defined as

$$\langle P_2(\cos\phi)\rangle = (3\langle\cos^2\phi\rangle - 1)/2 \tag{3}$$

The obtained $\langle P_2 \rangle$ for the processed Cell1.0-BA19.5kM-MA10.2k and Cell0.9-BA19.5kMMA13.4k are 0.34 and 0.41, respectively. The orientation parameter, $\langle P_2 \rangle$, increases with the molecular mass of the PMMA block (Figure 4c). Therefore, the orientation of the microstructures in the processed samples as detected by SAXS is indeed not so

weak as seen from these $\langle P_2 \rangle$ values. Due to the cyclic tensile deformation process, the microdomains in these bottlebrush copolymer elastomers are highly oriented and are preserved after the release of tensile stress. Eventually, the oriented nanofiber microstructures in the bottlebrush copolymer samples endow mimicking skin's mechanical properties. It is noted here that the PMMA block does play a key role in preserving the orientation of the nanofiber microstructures, which is attributed to the high $T_{\rm g}$ of the PMMA block. After the cyclic tensile deformation steps, the PMMA microdomains produce a plastic deformation that is permanent, resulting in oriented nanofiber microstructures.

Transmission electron microscopy (TEM) was further used to reveal the internal nanofiber microstructures of the processed bottlebrush Cell-g-PBA-b-PMMA copolymer elastomers. Figure 5 shows the typical TEM micrographs for

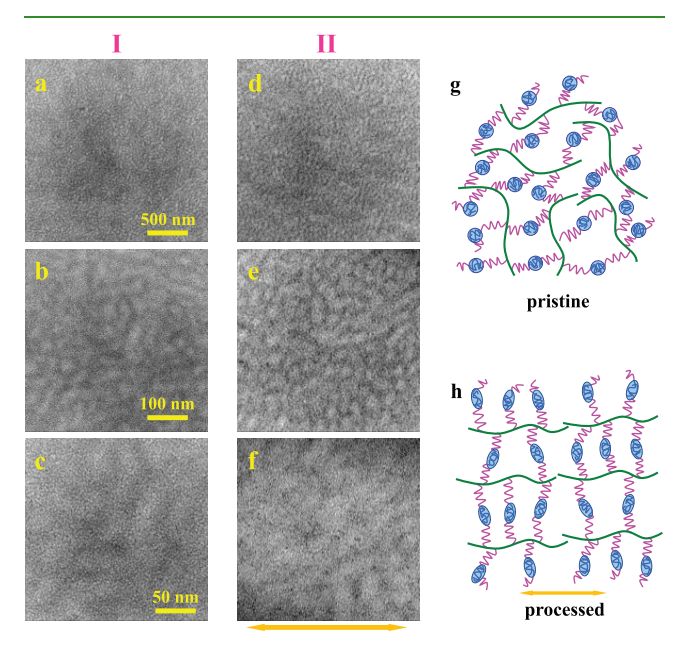


Figure 5. TEM micrographs and schematic illustration of the microstructures. Different TEM magnitudes for the processed bottlebrush copolymer Cello.9-BA19.5kMMA13.4k with observation perpendicular to the tensile direction (I) and parallel to the tensile direction (II). Schematic illustration of the microstructures for (g) pristine and (h) the processed bottlebrush Cell-g-PBA-b-PMMA copolymer elastomers. The yellow double-head arrow indicates the tensile direction.

Cell0.9-BA19.5kMMA13.4k. When perpendicular to the tensile direction, the TEM micrographs shown in Figure 5I do not show any obvious orientation for the cylinder-like microstructures. However, the TEM micrographs in Figure 5II do show two-sized microstructures that are perpendicular to the tensile direction. The large microdomains represent the cylinder structures for the bottlebrush copolymers and the small ones represent the nanofiber-like PMMA domains, which also correspond to the primary and secondary SAXS peaks (q_1 and q_2) in Figure 3. TEM micrograph for the pristine bottlebrush copolymer Cell0.9-BA19.5kMMA13.4k does not show obvious microdomain orientation (Figure S10), which is similar to that in Figure 5I.

According to SAXS and TEM results, the internal microstructures for the bottlebrush Cell-g-PBA-b-PMMA copolymer elastomers are proposed and illustrated in Figure 5g,h. On the

one hand, the cellulose backbone chain of the bottlebrush molecules confines the grafted side chains (PBA-b-PMMA diblocks) to the volume of a cylinder. On the other hand, microphase separation caused by the incompatibility of PBA and PMMA blocks results in self-assembling to form PMMA hard microdomains, which can serve as strong physical crosslinking points in the system. Prior to the tensile deformation (the pristine sample, Figure 5g), the large microdomains composed of bottlebrush molecules and the small PMMA hard microdomains are isotropically dispersed in the system, while after cyclic tensile deformation (the processed sample, Figure 5h), the cellulose backbones are aligned along the tensile direction. Due to the restriction of the grafted side chains of the diblock by cellulose backbones, the side chains prefer to orientate perpendicular to the tensile direction, so do the small nanofiber-like PMMA hard microdomains. Therefore, the large bottlebrush cylinder microdomains and the small PMMA microdomains are both aligned in the same direction perpendicular to the tensile direction, consistent with the appearance of SAXS arcs in the meridian direction shown in Figure 2.

SAXS and TEM results show that the cyclic tensile deformation induces anisotropic nanofiber structures. Similarly, the mechanical properties of the processed bottlebrush copolymers change to be anisotropic, and the monotonic nominal stress-strain curves in the machine direction and the transverse direction are illustrated in Figures S7-S9. The elongation at break in the transverse direction is longer than that in the machine direction of the processed bottlebrush Cell-g-PBA-b-PMMA copolymer elastomers. For Cell1.0-BA19.5kMMA10.2k and Cell0.9-BA19.5kMMA13.4k, the breaking strength in the transverse direction was lower than that in the machine direction, which was attributed to the oriented nanofiber PMMA domains and cellulose backbones. However, there is no orientation occurring in the system due to the good elastic recovery of Cell1.2-BA19.5kMMA4.7k, which resulted in little difference between the transverse and machine direction curves. This result is consistent with the microstructure of the skin because the mechanical properties of the skin are also anisotropic. The collagen fibers in the dermis are parallel to the direction of the Langer's line, and so the skin strength is high along the Langer's line and the skin perpendicular to the Langer's line can stretch longer. 12,13,45

CONCLUSIONS

In summary, we designed and synthesized reprocessable bottlebrush cellulose-graft-diblock copolymer elastomers (cellulose-graft-poly(n-butyl acrylate)-b-poly(methyl methacrylate), Cell-g-PBA-b-PMMA), which would be able to perfectly mimic the mechanical properties of human and animal skins. Thermogravimetric analysis (TGA) showed that these elastomers had sufficient thermal stability, providing a fundamental basis for future practical applications. The immiscibility of the two components PBA and PMMA in the grafted side chains led to self-assembly of PMMA, which finally formed physical crosslinking points, enabling the vast increase of tensile strength of the elastomers. These processable bottlebrush copolymer elastomers allowed forming objects with desired shapes, which was essential for elastomer recycling, impossible in chemically cross-linked networks. Furthermore, by step-cyclic mechanical processing simply at room temperature, the mechanical behavior of the processed bottlebrush Cell-g-PBA-b-PMMA copolymer elastomers could

amazingly behave very similar to that of human and animal skins. The hard PMMA and soft PBA microdomains acted likely as the rigid and elastic components in skins, endowing the elastomers with sufficient tensile strength and elasticity. The complementary small-angle X-ray scattering (SAXS) and transmission electron microscopy (TEM) both together verified the orientation of the internal nanofiber microstructures in the processed elastomers, making it possible that after simple step-cyclic tensile deformation, the bottle-brush Cell-g-PBA-b-PMMA copolymer elastomers could exhibit similar mechanical behaviors to those of skin. These materials are essential to advance the future development of biomimetic polymer materials.

ASSOCIATED CONTENT

3 Supporting Information

The Supporting Information is available free of charge at https://pubs.acs.org/doi/10.1021/acsami.0c21494.

Additional TGA and DTG curves, monotonic nominal stress-strain curves, GPC traces, SAXS intensity profiles, TEM micrograph and ¹H NMR spectrum (PDF)

AUTHOR INFORMATION

Corresponding Authors

Sergei S. Sheiko — Department of Chemistry, University of North Carolina at Chapel Hill, Chapel Hill, North Carolina 27599, United States; oorcid.org/0000-0003-3672-1611; Email: sergei@email.unc.edu

Xuehui Wang — CAS Key Laboratory of Soft Matter Chemistry, Department of Polymer Science and Engineering, University of Science and Technology of China, Hefei, Anhui 230026, China; Email: xhwang01@ustc.edu.cn

Zhigang Wang — CAS Key Laboratory of Soft Matter Chemistry, Department of Polymer Science and Engineering, University of Science and Technology of China, Hefei, Anhui 230026, China; orcid.org/0000-0002-6090-3274; Email: zgwang2@ustc.edu.cn

Authors

Juan Zhang – CAS Key Laboratory of Soft Matter Chemistry, Department of Polymer Science and Engineering, University of Science and Technology of China, Hefei, Anhui 230026, China

Andrew N. Keith — Department of Chemistry, University of North Carolina at Chapel Hill, Chapel Hill, North Carolina 27599, United States; orcid.org/0000-0001-6351-5392

Complete contact information is available at: https://pubs.acs.org/10.1021/acsami.0c21494

Author Contributions

J.Z. and Z.W. conceived and designed the project and experiments; J.Z. performed the materials fabrication, characterizations, data analysis, and discussed the results; X.W. and Z.W. supervised the entire project; J.Z. and Z.W. wrote the manuscript; A.N.K. and S.S.S. performed the data analysis and discussion. All authors discussed the results and commented on the manuscript.

Notes

The authors declare no competing financial interest.

ACKNOWLEDGMENTS

The authors acknowledge financial support from the National Natural Science Foundation of China (Grant 51673183 and 52073266) and the Open Research Fund of State Key Laboratory of Polymer Physics and Chemistry, Changchun Institute of Applied Chemistry, Chinese Academy of Sciences. The BL16B1 beamline at Shanghai Synchrotron Radiation Facility offers support for end-users to carry out SAXS measurements.

REFERENCES

- (1) Lackner, J. M.; Waldhauser, W.; Major, R.; Major, L.; Hartmann, P. Biomimetics in Thin Film Design-Wrinkling and Fracture of Pulsed Laser Deposited Films in Comparison to Human Skin. *Surf. Coat. Technol.* **2013**, *215*, 192–198.
- (2) Lei, Z.; Wu, P. A Supramolecular Biomimetic Skin Combining a Wide Spectrum of Mechanical Properties and Multiple Sensory Capabilities. *Nat. Commun.* **2018**, *9*, No. 1134.
- (3) Giacomo, R. D.; Bonanomi, L.; Costanza, V.; Maresca, B.; Daraio, C. Biomimetic Temperature-Sensing Layer for Artificial Skins. *Sci. Robot.* **2017**, *2*, No. eaai9251.
- (4) Wen, L.; Weaver, J. C.; Lauder, G. V. Biomimetic Shark Skin: Design, Fabrication and Hydrodynamic Function. *J. Exp. Biol.* **2014**, 217, 1656–1666.
- (5) Xu, L. Z.; Zhao, X. L.; Xu, C. L.; Kotov, N. A. Water-Rich Biomimetic Composites with Abiotic Self-Organizing Nanofiber Network. *Adv. Mater.* **2018**, *30*, No. 1703343.
- (6) Gur, D.; Leshem, B.; Oron, D.; Werner, S.; Addadi, L. The Structural Basis for Enhanced Silver Reflectance in Koi Fish Scale and Skin. *J. Am. Chem. Soc.* **2014**, *136*, 17236–17242.
- (7) Bhushan, B. Biomimetics: Lessons From Nature-An Overview. *Philos. Trans. R. Soc., A* **2009**, *367*, 1445–1486.
- (8) Jussila, J.; Leppaniemi, A.; Paronen, M.; Kulomaki, E. Ballistic skin simulant. *Forensic Sci. Int.* **2005**, *150*, 63–71.
- (9) Kim, J.; Lee, M.; Shim, H. J.; Ghaffari, R.; Cho, H. R.; Son, D.; Jung, Y. H.; Soh, M.; Choi, C.; Jung, S.; Chu, K.; Jeon, D.; Lee, S. T.; Kim, J. H.; Choi, S. H.; Hyeon, T.; Kim, D. H. Stretchable Silicon Nanoribbon Electronics for Skin Prosthesis. *Nat. Commun.* **2014**, *5*, No. 5747.
- (10) Sun, J. Y.; Keplinger, C.; Whitesides, G. M.; Suo, Z. Ionic Skin. *Adv. Mater.* **2014**, *26*, 7608–7614.
- (11) Chortos, A.; Liu, J.; Bao, Z. Pursuing Prosthetic Electronic Skin. *Nat. Mater.* **2016**, *15*, 937–950.
- (12) Joodaki, H.; Panzer, M. B. Skin Mechanical Properties and Modeling: A Review. *Proc. Inst. Mech. Eng., Part H* **2018**, 232, 323–343.
- (13) Wong, W. L.; Joyce, T. J.; Goh, K. L. Resolving the Viscoelasticity and Anisotropy Dependence of The Mechanical Properties of Skin From a Porcine Model. *Biomech. Model. Mechanobiol.* **2016**, *15*, 433–446.
- (14) Kendall, M. A.; Chong, Y. F.; Cock, A. The Mechanical Properties of The Skin Epidermis in Relation to Targeted Gene and Drug Delivery. *Biomaterials* **2007**, *28*, 4968–4977.
- (15) Meijer, R.; Douven, L. F.; Oomens, C. W. Characterisation of Anisotropic and Non-Linear Behaviour of Human Skin in Vivo. *Comput. Methods Biomech. Biomed. Eng.* **1999**, *2*, 13–27.
- (16) Escoffier, C.; de Rigal, J.; Rochefort, A.; Vasselet, R.; Lévêque, J. L.; Agache, P. G. Age-Related Mechanical Properties of Human Skin: An in Vivo Study. *J. Invest. Dermatol.* **1989**, *93*, 353–357.
- (17) Rabiei, R.; Dastjerdi, A. K.; Mirkhalaf, M.; Barthelat, F. Hierarchical Structure, Mechanical Properties and Fabrication of Biomimetic. *Biomater. Biomimetic Biomater.* **2013**, 67–90.
- (18) Silver, F. H.; Siperko, L. M.; Seehra, G. P. Mechanobiology of Force Transduction in Dermal Tissue. *Skin Res. Technol.* **2003**, *9*, 3–23.

- (19) Silver, F. H.; Freeman, J. W.; Devore, D. Viscoelastic Properties of Human Skin and Processed Dermis. *Skin Res. Technol.* **2001**, *7*, 18–23.
- (20) Hendriks, F. M.; Brokken, D.; Eemeren, J. T. W. M. V.; Oomens, C. W. J.; Baaijens, F. P. T.; Horsten, J. B. A. M. A Numerical-Experimental Method to Characterize the Non-Linear Mechanical Behaviour of Human Skin. Skin Res. Technol. 2003, 9, 274–283.
- (21) Annaidh, A. N.; Bruyere, K.; Destrade, M.; Gilchrist, M. D.; Ottenio, M. Characterization of the Anisotropic Mechanical Properties of Excised Human Skin. *J. Mech. Behav. Biomed. Mater.* **2012**, *5*, 139–48.
- (22) Dunn, M. G.; Silver, F. H. Viscoelastic Behavior of Human Connective Tissues: Relative Contribution of Viscous and Elastic Components. *Connect. Tissue Res.* **1983**, *12*, 59–70.
- (23) Dorrington, K. L.; McCrum, N. G. Elastin as a Rubber. *Biopolymers* 1977, 16, 1201–1222.
- (24) Cotta-Pereira, G.; Rodrigo, G.; Bittencourt-Sampaio, S. Oxytalan, Elaunin, and Elastic Fibers in the Human Skin. *J. Invest. Dermatol.* **1976**, *66*, 143–148.
- (25) Dąbrowska, A. K.; Rotaru, G. M.; Derler, S.; Spano, F.; Camenzind, M.; Annaheim, S.; Stampfli, R.; Schmid, M.; Rossi, R. M. Materials Used to Simulate Physical Properties of Human Skin. *Skin Res. Technol.* **2016**, *22*, 3–14.
- (26) Jachowicz, J.; McMullen, R.; Prettypaul, D. Indentometric Analysis of in Vivo Skin and Comparison with Artificial Skin Models. *Skin Res. Technol.* **2007**, *13*, 299–309.
- (27) Elleuch, K.; Elleuch, R.; Zahouani, H. Comparison of Elastic and Tactile Behavior of Human Skin and Elastomeric Materials Through Tribological Tests. *Polym. Eng. Sci.* **2006**, *46*, 1715–1720.
- (28) Wang, Z. K.; Yuan, L.; Jiang, F.; Zhang, Y. Q.; Wang, Z. G.; Tang, C. B. Bioinspired High Resilient Elastomers to Mimic Resilin. ACS Macro Lett. 2016, 5, 220–223.
- (29) Abbasi, M.; Faust, L.; Wilhelm, M. Comb and Bottlebrush Polymers with Superior Rheological and Mechanical Properties. *Adv. Mater.* **2019**, *31*, No. 1806484.
- (30) Jiang, F.; Wang, Z. K.; Qiao, Y. L.; Wang, Z. G.; Tang, C. B. A Novel Architecture Toward Third-Generation Thermoplastic Elastomers by a Grafting Strategy. *Macromolecules* **2013**, *46*, 4772–4780.
- (31) Daniel, W. F.; Burdynska, J.; Vatankhah-Varnoosfaderani, M.; Matyjaszewski, K.; Paturej, J.; Rubinstein, M.; Dobrynin, A. V.; Sheiko, S. S. Solvent-Free, Supersoft and Superelastic Bottlebrush melts and Networks. *Nat. Mater.* **2016**, *15*, 183–189.
- (32) Verduzco, R.; Li, X. Y.; Pesek, S. L.; Stein, G. E. Structure, function, Self-Assembly, and Applications of Bottlebrush Copolymers. *Chem. Soc. Rev.* **2015**, *44*, 2405–2420.
- (33) Zhang, J.; Wang, Z. K.; Wang, X. H.; Wang, Z. G. The Synthesis of Bottlebrush Cellulose-*graft*-Diblock Copolymer Elastomers via Atom Transfer Radical Polymerization Utilizing a Halide Exchange Technique. *Chem. Commun.* **2019**, *55*, 13904–13907.
- (34) Xie, G.; Martinez, M. R.; Olszewski, M.; Sheiko, S. S.; Matyjaszewski, K. Molecular Bottlebrushes as Novel Materials. *Biomacromolecules* **2019**, 20, 27–54.
- (35) Schmelz, J.; Schedl, A. E.; Steinlein, C.; Manners, I.; Schmalz, H. Length Control and Block-Type Architectures in Worm-Like Micelles with Polyethylene Cores. *J. Am. Chem. Soc.* **2012**, *134*, 14217–14225.
- (36) Vatankhah-Varnosfaderani, M.; Keith, A. N.; Cong, Y.; Liang, H.; Rosenthal, M.; Sztucki, M.; Clair, C.; Magonov, S.; Ivanov, D. A.; Dobrynin, A. V.; et al. Chameleon-Like Elastomers with Molecularly Encoded Strain-Adaptive Stiffening and Coloration. *Science* **2018**, *359*, 1509–1513.
- (37) Wang, Z. K.; Jiang, F.; Zhang, Y. Q.; You, Y. Z.; Wang, Z. G.; Guan, Z. B. Bioinspired Design of Nanostructured Elastomers with Cross-Linked Soft Matrix Grafting on the Oriented Rigid Nanofibers to Mimic Mechanical Properties of Human Skin. ACS Nano 2015, 9, 271–278.
- (38) Keith, A. N.; Vatankhah-Varnosfaderani, M.; Clair, C.; Fahimipour, F.; Dashtimoghadam, E.; Lallam, A.; Sztucki, M.;

- Ivanov, D. A.; Liang, H.; Dobrynin, A. V.; Sheiko, S. S. Bottlebrush Bridge Between Soft Gels and Firm Tissues. *ACS Cent. Sci.* **2020**, *6*, 413–419.
- (39) Wang, Z. G.; Niu, Y. H.; Fredrickson, G. H.; Kramer, E. J.; Shin, Y. W.; Shimizu, F.; Zuo, F.; Rong, L.; Hsiao, B. S.; Coates, G. W. Step-Cycle Mechanical Processing of Gels of sPP-b-EPR-b-sPP Triblock Copolymer in Mineral Oil. *Macromolecules* **2010**, 43, 6782–6788.
- (40) Jansen, L. H.; Rottier, P. B. Some Mechanical Properties of Human Abdominal Skin Measured on Excised Strips. *Dermatology* **1958**, *117*, 65–83.
- (41) Greven, H.; Zanger, K.; Schwinger, G. Mechanical Properties of the Skin of *Xenopus laevis* (Anura, Amphibia). *J. Morphol.* **1995**, 224, 15–22
- (42) Grear, M. E.; Motley, M. R.; Crofts, S. B.; Witt, A. E.; Summers, A. P.; Ditsche, P. Mechanical Properties of Harbor Seal Skin and Blubber A Test of Anisotropy. *Zoology* **2018**, *126*, 137–144.
- (43) Ankersen, J.; Birkbeck, A. E.; Thomson, R. D.; Vanezis, P. Puncture Resistance and Tensile Strength of Skin Simulants. *Proc. Inst. Mech. Eng., Part H* 1999, 213, 493–501.
- (44) Shergold, O. A.; Fleck, N. A.; Radford, D. The Uniaxial Stress Versus Strain Response of Pig Skin and Silicone Rubber at Low and High Strain Rates. *Int. J. Impact Eng.* **2006**, *32*, 1384–1402.
- (45) Dobrynin, A. V.; Carrillo, J. M. Y. Universality in Nonlinear Elasticity of Biological and Polymeric Networks and Gels. *Macromolecules* **2011**, *44*, 140–146.
- (46) Mullins, L. Softening of Rubber by Deformation. Rubber Chem. Technol. 1969, 42, 339–362.
- (47) Men, Y.; Rieger, J.; Strobl, G. Role of the Entangled AmorPhous Network in Tensile Deformation of Semicrystalline Polymers. *Phys. Rev. Lett.* **2003**, *91*, No. 095502.
- (48) Wang, Z. G.; Xia, Z. Y.; Yu, Z. Q.; Chen, E. Q.; Sue, H. J.; Han, C. C.; Hsiao, B. S. Lamellar Formation and Relaxation in Simple Sheared Poly(ethylene terephthalate) by Small-Angle X-Ray Scattering. *Macromolecules* **2006**, *39*, 2930–2939.
- (49) Szewciw, L.; Barthelat, F. J. Mechanical Properties of Striped Bass Fish Skin: Evidence of an Exotendon Function of the Stratum Compactum. *Mech. Behav. Biomed. Mater.* **2017**, *73*, 28–37.